Journal of Applied Polymer Science

Controlling micro- and nanofibrillar morphology of polymer blends in low-speed melt spinning process. Part III: Fibrillation mechanism of PLA/PVA blends along the spinline

Nguyen Hoai An Tran,[1,2] Harald Brünig,[1] Maria Auf der Landwehr,[1] Gert Heinrich[1,3]

[1]Leibniz-Institut für Polymerforschung Dresden e. V, Dresden 01069, Germany

[2]Ho Chi Minh City University of Technology, VNU-HCM, Ho Chi Minh City, Vietnam

[3]Institut für Werkstoffwissenschaft, Technische Universität Dresden, Dresden 01062, Germany

Correspondence to: N. H. A. Tran (E-mail: tnhoaian@gmail.com) and H. Brünig (E-mail: bruenig@ipfdd.de)

ABSTRACT: The effects of spinning conditions on the fibrillation process of poly(lactic acid) (PLA) and poly(vinyl alcohol) (PVA) polymer blends in an elongational flow within the fiber formation zone are systematically and thoroughly investigated. By considering the relationship between the changes in filament parameters with the focus on the maximum axial strain rate (ASR) and tensile stress at maximum ASR and the morphological evolution of the dispersed PLA phase along the spinline, the fibrillation process from rod-like to nanofibrillar structures of the dispersed PLA phase in a binary blend with PVA matrix is elucidated. The final morphology of the dispersed PLA phase in PLA/PVA blends is controlled by the changes in the spinning conditions. The lengths and diameters of the PLA fibrils are caused not only by the deformation of their initial sizes but also by the combination of the deformation, coalescence, and break-up process. © 2016 Wiley Periodicals, Inc. J. Appl. Polym. Sci. **2016**, *133*, 44259.

KEYWORDS: extrusion rate; fibers; fibrillation process; flow rate; morphology; nanofibrillar morphology; shear flow; textiles; theory and modeling; thermoplastics

Received 1 June 2016; accepted 1 August 2016

DOI: 10.1002/app.44259

INTRODUCTION

The understanding of the formation of micro- and nanofibrillar structures of polymer blends within the fiber formation zone in the melt spinning process came recently into the focus of considerable academic and industrial interest because it helps tailoring and controlling the final morphology of the dispersed phase in polymer blends.[1–3] Recently, in our study,[4] we found that during melt spinning under specific spinning conditions (take-up velocity of 50 m min^{-1} and mass flow rate of 1.0 g min^{-1}) the morphology of the dispersed poly(lactic acid) (PLA) phase was changed from rod-like micro-scale structures into continuous long nanofibrils within the fiber formation zone. It was found that the axial strain rate (ASR) and tensile stress is considered as the two most important factors that led to the deformation of the dispersed PLA phase in PLA/PVA blend extrudates.

More recently,[5] by changing the spinning conditions like take-up velocity and flow rate, the profile of filament velocity, diameter, tensile stress, and apparent elongational viscosity along the spinline are different, except the filament temperature profiles are nearly the same for various take-up velocities at the constant mass flow rate. It was also found that the maximum ASR and the tensile stress at maximum ASR decrease with increasing of flow rate at constant take-up velocity and these both quantities increase with increasing take-up velocity at constant flow rate.

The present article, as the third part of our current investigations, demonstrates the morphological development of PLA/PVA-filaments in both longitudinal and cross-sectional directions at different locations within the fiber formation zone along the spinline (Figure 1, Positions P1 to P8) for various spinning conditions (Table I). Comparing this morphological evolution of PLA/PVA-filaments with all filament parameter profiles, especially with the maximum ASR and tensile stress at ASR as presented in our previous study,[5] various possible conceptual models for the fibrillation process of the dispersed PLA phase, depending on the spinning conditions and the droplet sizes, are proposed.

This article will also answer several questions related to the mechanism of the fibrillation process and controlling the micro-and nanofibrillar structures of the dispersed PLA phase in PLA/PVA-filaments (see ref. 5). The findings of the current study provide a systematical and thorough insight into the mechanism of the fibrillation process of polymer blends within fiber formation zone

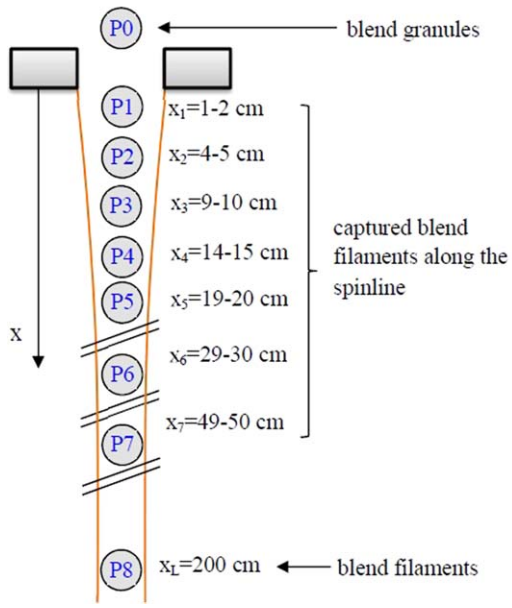

Figure 1. Schematic view of a monofilament and locations P1 to P8 of the captured samples. It is worth remembered that the morphological changes of PLA/PVA-blends at Position 0 (P0) through a convergent capillary die were investigated in our previous publication.[6] [Color figure can be viewed at wileyonlinelibrary.com.]

in the melt spinning process and present basic requirements for producing and controlling micro- and nanofibrillar PLA structures using a conventional melt spinning process.

EXPERIMENTAL

Materials, Melt Mixing, and Melt Spinning

The materials (PLA 6020D and PVA Mowiflex TC 232), the melt mixing using twin-screw extruder, and the melt spinning on the piston-type melt spinning device are fully described in our previous publications.[4–6]

Table I represents the spinning conditions for the melt spinning processes. For instant, the take-up velocity is altered from 10 to 70 m min^{-1} at a constant mass flow rate of 1.0 g min^{-1} and the mass flow rate is also changed at a constant take-up velocity of 50 m min^{-1}.

Table I. Spinning Conditions[5]

Conditions	Take-up velocity (m min^{-1})	Volumetric flow rate (cm^3 min^{-1})	Mass flow rate (g min^{-1})
A	50	0.393	0.5
		0.785	1.0
		1.178	1.5
		1.570	2.0
B	10		
	30	0.785	1.0
	50		
	70		

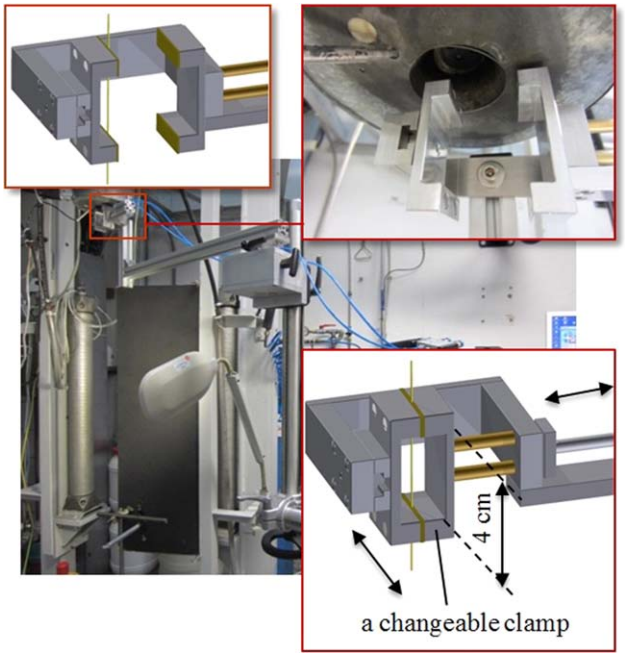

Figure 2. Fiber-capturing device at IPF Dresden e. V. [Color figure can be viewed at wileyonlinelibrary.com.]

Morphology Characterization

Sample Preparations. Pieces having 4 cm long PLA/PVA-filaments were collected using a self-constructed fiber-capturing device which was fabricated in our own machine shop at IPF Dresden e. V. (Figure 2). The device is mounted on a platform that can be moved vertically over distances ranging from 2 cm to 150 cm from the die exit to capture the running filament at different locations along the spinline. The fiber capturing device consists of several changeable clamps and it is automatically operated by compressed air. The molten polymer filament is caught very fast within 0.01 s and is instantly quenched and solidified as soon as it was trapped by surrounding air at room temperature of 25 °C without any additional cooling medium.

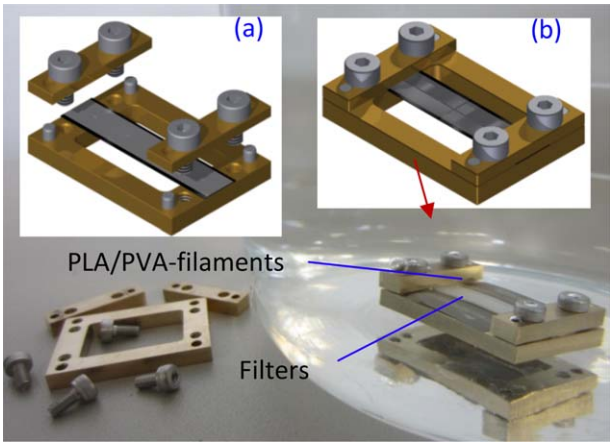

Figure 3. PVA removing process in distiller water: PLA/PVA-filaments were fixed in filament-keeping device (a and b), then were immersed in water for 24 h. [Color figure can be viewed at wileyonlinelibrary.com.]

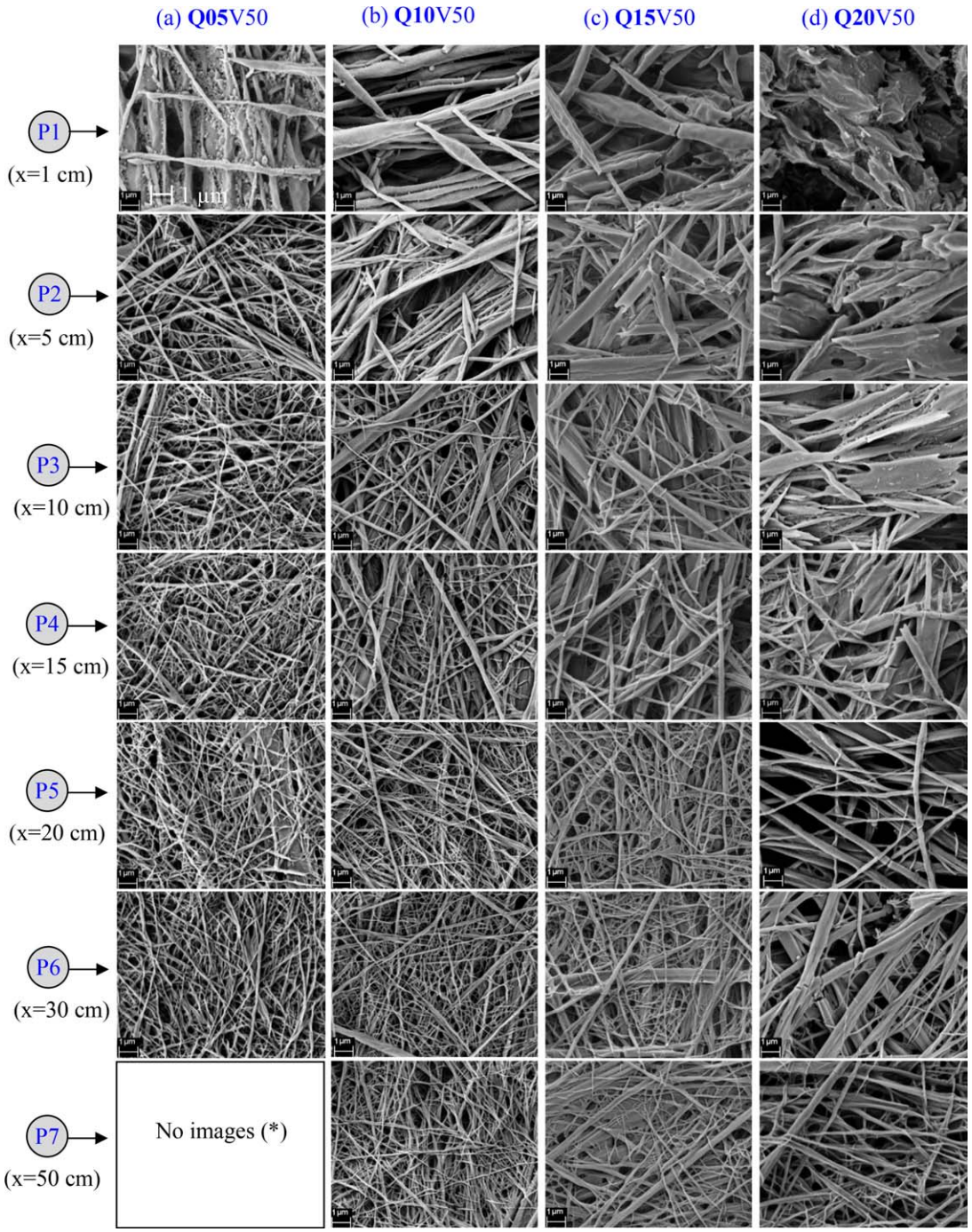

Figure 4. SEM images of the dispersed PLA phase after removing the PVA matrix for the various mass flow rates (0.5–2.0 g min^{-1}) (Q05–Q20) and the constant take-up velocity of 50 m min^{-1} (V50) (Q05V50, Q10V50, Q15V50, Q20V50) at different locations (P1–P7) along the spinline: scale bar is 1 µm, (*) Experiments were not done at this location because it was supposed that there is no difference in PLA morphology at this location with that at x = 30 cm (P6). [Color figure can be viewed at wileyonlinelibrary.com.]

The solidified pieces of PLA/PVA-filaments between the clamps are then ready to investigate their morphological properties.

A similar fiber capturing device has already been used to cut a specific fiber length for calculation of the linear density of fiber by Kase and Matsuo[7] and determination of the fiber diameter by Ishibashi *et al.*[8] and Oh.[9]

Two kinds of PLA/PVA-filament samples were prepared to study their morphology: The PLA/PVA blend fragments 1 cm long were cut from the middle of the captured PLA/PVA-filaments 4 cm long and the PLA/PVA blend fragments were fractured at the middle of the captured PLA/PVA-filaments 4 cm long in liquid nitrogen. The latter was prepared to investigate the cross-sectional morphology of the captured PLA/PVA-filaments.

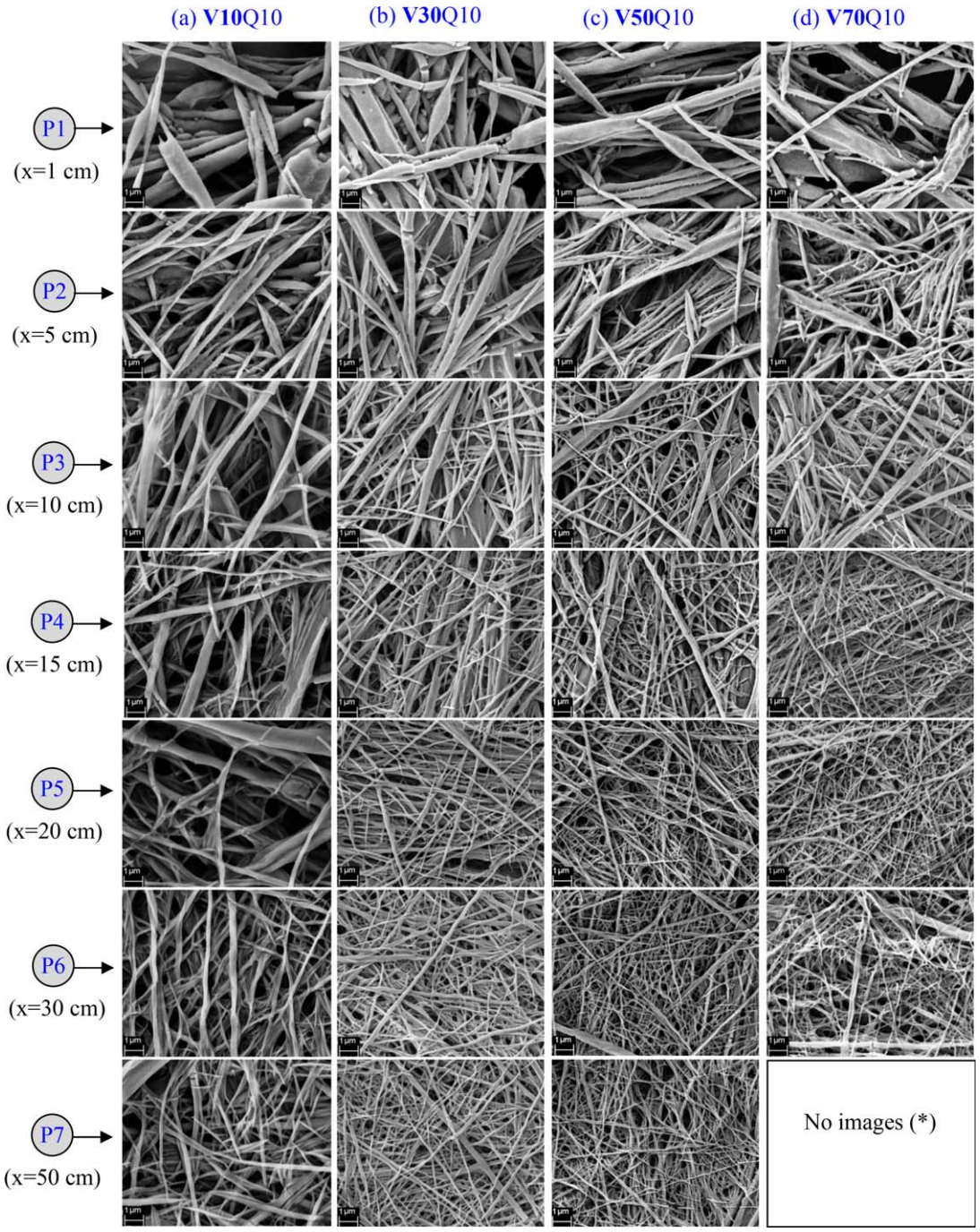

Figure 5. SEM images of the dispersed PLA phase after removing the PVA matrix for various take-up velocities (10–70 m min^{-1}) (V10–70) and the constant mass flow rate of 1.0 g min^{-1} (Q10) (V10Q10, V30Q10, V50Q10, V70Q10) at different locations (P1–P7) along the spinline: scale bar is 1 μm, (*)Experiments were not done at this location because it was supposed that there is no difference in PLA morphology at this location with that at x = 30 cm (P6). [Color figure can be viewed at wileyonlinelibrary.com.]

These blend samples were immersed in chloroform for 8 h at 50 °C and in distilled water for 24 h at room temperature (ca. 25 °C) to remove the dispersed PLA phase and the PVA matrix material, respectively. In the latter case, the remaining dispersed PLA phase after removing the PVA matrix is unstable during removing process. Therefore, the self-fabricated filament keeping device was used to fix the captured PLA/PVA-filaments, which are laid on flat filter paper or filter stainless metal during removing the PVA matrix in water for 24 h (Figure 3).

Scanning Electron Microscopy. After etching the dispersed PLA phase or removing the PVA matrix from PLA/PVA-filament samples, the remaining phase was dried at room temperature for 24 h. All dried samples were investigated using scanning

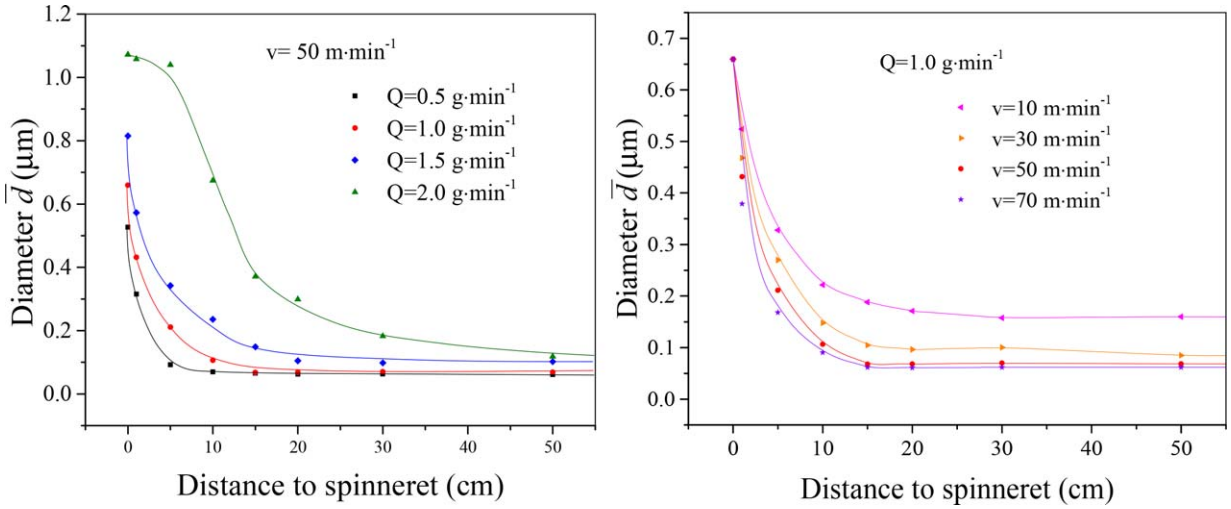

Figure 6. Mean diameter $\bar{d}$ of the dispersed PLA phase after removing the PVA matrix vs. distance. [Color figure can be viewed at wileyonlinelibrary.com.]

electron microscopy (SEM) Ultra Plus (Carl Zeiss NTS GmbH, Oberkochen, Germany). The sample discs were prepared by sputtering a thin layer of 3 nm platinum.

RESULTS AND DISCUSSION

Residual PLA Fibrils after Removing PVA Matrix

Figures 4 and 5 present the SEM images of the PLA morphology after removing the PVA matrix from PLA/PVA-filaments at different locations (P1–P7) along the spinline for different spinning conditions. Figure 6 plots the mean diameter of the dispersed PLA phase $\bar{d}$ versus distance to spinneret (also see Figure A.1 in Appendix). It is obviously seen that the dispersed PLA phase is deformed from short rod-like or ellipsoidal structures in micro-scale into longer fibrillar structures in nano-scale along the spinline for all spinning conditions. For spinning condition A, in which the take-up velocity is constant, the mean diameter of the dispersed PLA phase $\bar{d}$ decreases much faster at the low mass flow rate $Q = 0.5$ g min^{-1} than that of higher mass flow rates $Q = 1.0$, 1.5, and 2.0 g min^{-1} [Figure 6(a)]. For spinning condition B, in which the mass flow rate is constant, the mean diameter $\bar{d}$ decreases faster at the high take-up velocity $v = 70$ m min^{-1} than that of lower take-up velocities $v = 10$, 30, and 50 m min^{-1} [Figure 6(b)]. These results indicate that the above defined spinning conditions have a profound impact on the deformation of the dispersed PLA phase in PLA/PVA-filaments. It was found that under each spinning condition, the profile of filament velocity, temperature, tensile stress, and apparent elongational viscosity along the spinline are different as presented in our previous article.[5] Except the filament temperature profiles are nearly the same for various take-up velocities at the constant mass flow rate of 1.0 g min^{-1}. Among these filament parameters, the ASR (including local and maximum ASR) and the tensile stress are considered as the two most important factors that lead to the deformation of the dispersed PLA phase in PLA/PVA-filament.

Table II lists the maximum ASR, tensile stress at maximum ASR, and their location to spinneret for different spinning conditions. Figure 7 plots the maximum ASR value and its locations versus mass flow rate and take-up velocity. It is seen from Figure 7 that the maximum ASR almost linearly decreases with the increase of mass flow rate at the constant take-up velocity and it is linearly proportional to take-up velocity for the

Table II. Maximum Axial Strain Rate (ASR) and its Locations for Different Spinning Conditions

Conditions	Take-up velocity (m min^{-1})	Mass flow rate (g min^{-1})	Maximum ASR (s^{-1})	Distance to spinneret (cm)	Tensile stress at max ASR (MPa)
A	50	0.5	10.61	7.5	1.73
		1.0	7.67	10	0.52
		1.5	3.03	15	0.39
		2.0	2.28	15	0.25
B	10		1.23	7.5	0.18
	30	1.0	2.59	10	0.35
	50		7.67	10	0.52
	70		9.07	10	0.74

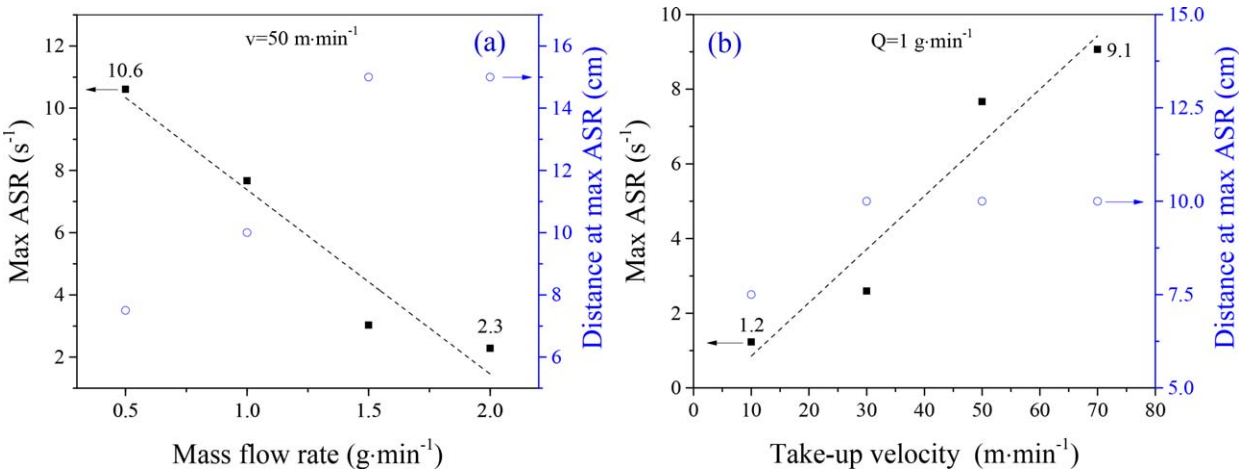

Figure 7. Maximum ASR and the position of maximum ASR vs. mass flow rate (a) and take-up velocity (b). [Color figure can be viewed at wileyonlinelibrary.com.]

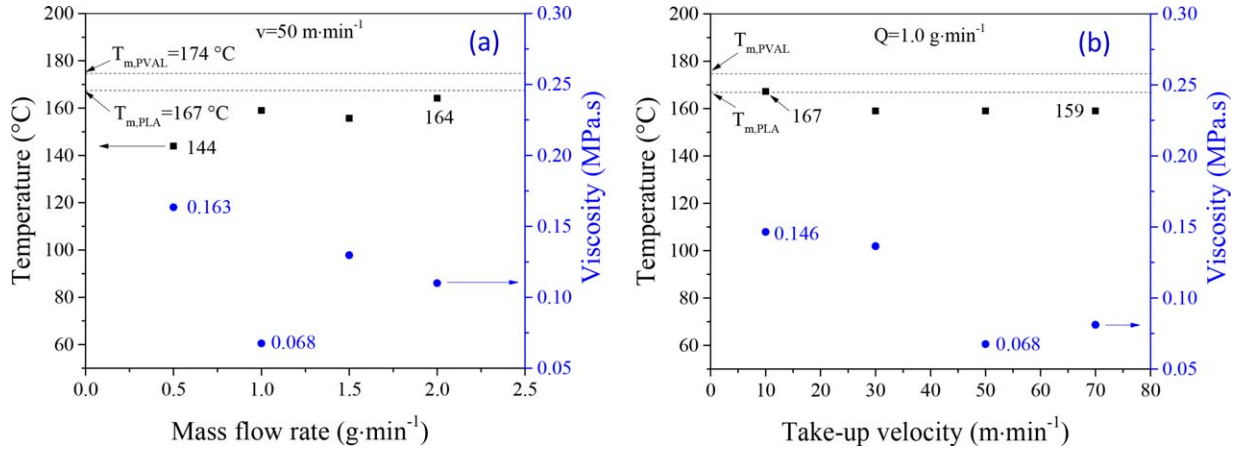

Figure 8. Temperature and apparent elongational viscosity of filament at maximum ASR vs. mass flow rate (a) and take-up velocity (b). [Color figure can be viewed at wileyonlinelibrary.com.]

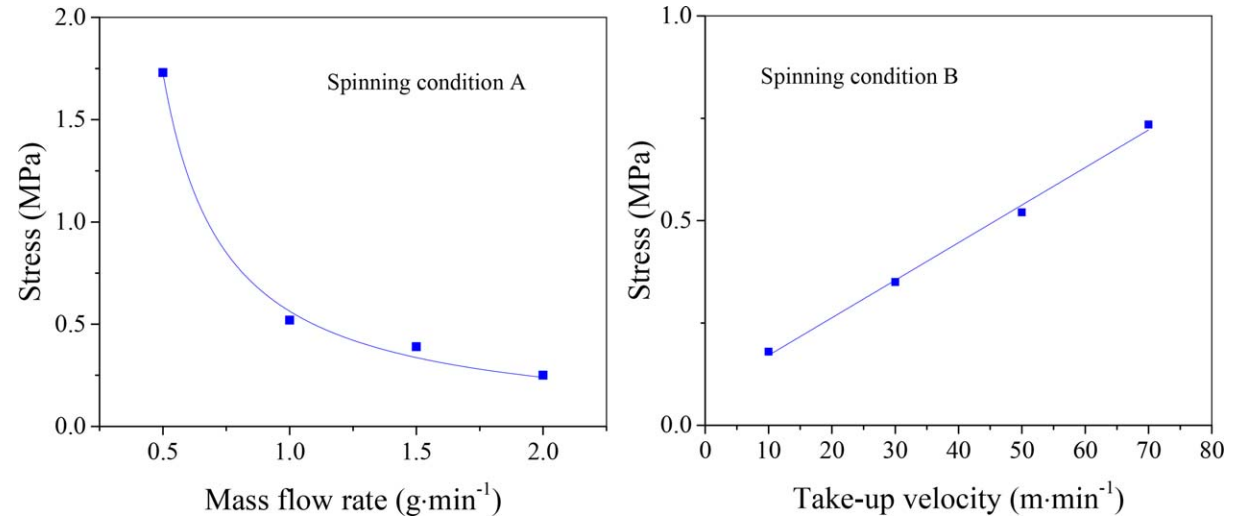

Figure 9. Tensile stress at maximum ASR for different spinning conditions A (a) and B (b). [Color figure can be viewed at wileyonlinelibrary.com.]

Table III. Average Diameters $\bar{d}$ of the PLA Fibrils after Removing the PVA Matrix at Locations P6 $\bar{d}_{x30}$ ($x = 30$ cm), P7 $\bar{d}_{x50}$ ($x = 50$ cm), and P8 $\bar{d}_L$ ($x = 200$ cm)

Conditions	Take-up velocity v (m min^{-1})	Mass flow rate Q (g min^{-1})	$\bar{d}_{x30}$ or $\bar{d}_{x50}$ (μm)	x_{30} or x_{50} (cm)	$\bar{d}_L(x_L = 200$ cm) (μm)
A	50	0.5	0.062	30	0.061
		1.0	0.068	50	0.067
		1.5	0.102	50	0.089
		2.0	0.119	50	0.092
B	10		0.160	50	0.148
	30	1.0	0.085	50	0.084
	50		0.068	50	0.067
	70		0.062	30	0.062

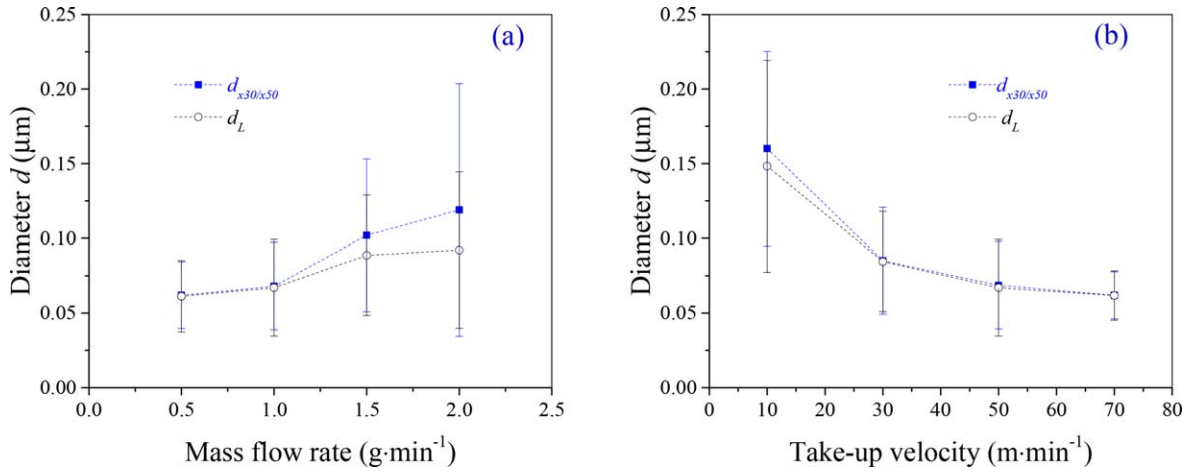

Figure 10. Average diameter of PLA fibrils at P6 (x = 30 cm) $\bar{d}_{x30}$, P7 (x = 50 cm) $\bar{d}_{x50}$, and P8 $\bar{d}_L$ (xL = 200 cm) vs. mass flow rate (a) and take-up velocity (b). [Color figure can be viewed at wileyonlinelibrary.com.]

constant mass flow rate. Comparing these results with the SEM images in Figures 4 and 5, and with diagrams in Figure 6 reveals that an increase in the maximum ASR value, i.e. the decrease of mass flow rate at constant take-up velocity or the increase of take-up velocity at constant mass flow rate, causes a significant decrease in the final size of the dispersed PLA phase.

All the filament parameters at maximum ASR, which were discussed in our previous article,[5] should be now reconsidered. It was found that the filament temperature at maximum ASR goes just below

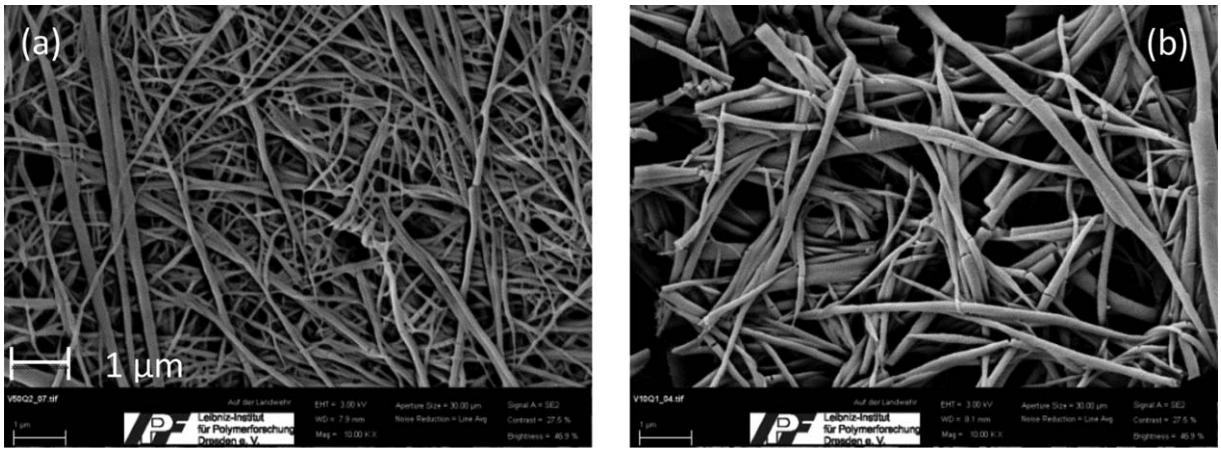

Figure 11. SEM images of the dispersed PLA phase from PLA/PVA-filaments at P8 for the two special spinning conditions: Q = 2.0 g min^{-1} and v = 50 m min^{-1} (a), v = 10 m min^{-1} and Q = 1.0 g min^{-1} (b). Scale bar: 1 μm.

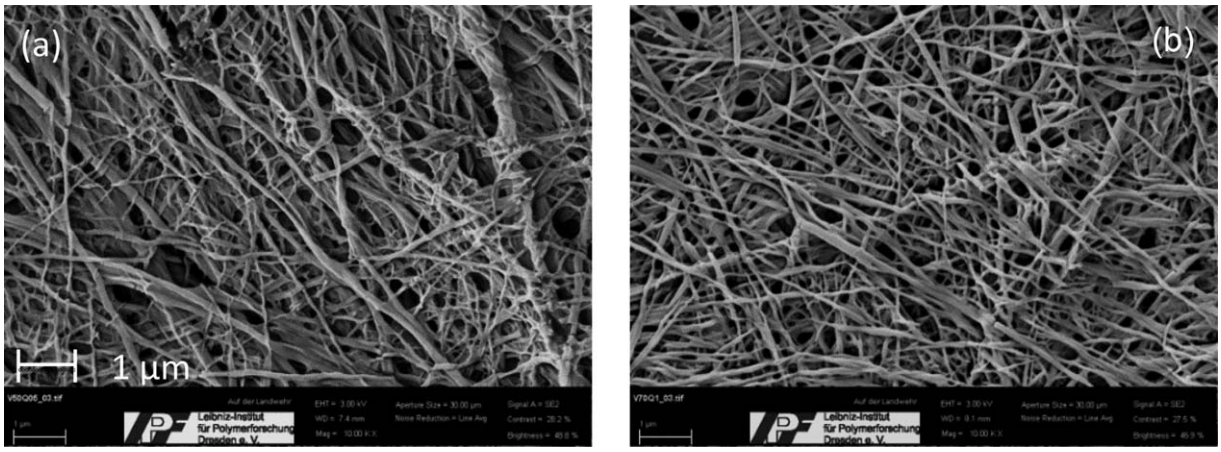

Figure 12. SEM images of the dispersed PLA phase from PLA/PVA-filaments at P8 for the two limiting spinning conditions: Q = 0.5 g min^{-1} and v = 50 m min^{-1} (a), v = 70 m min^{-1} and Q = 1.0 g min^{-1} (b). Scale bar: 1 µm.

melting temperature of PLA $T_{m,PLA}$ and it is much higher than its glass transition temperature (Figure 8). At this location, the apparent elongational viscosity had a value either equal or slightly higher than its minimum value. Thus, the filament state at maximum ASR is under the best conditions for the filament deformation.

Figure 9 plots the tensile stress at maximum ASR versus mass flow rate and take-up velocity. It is seen that tensile stress at maximum ASR decreases with the increase of the mass flow rate at the constant take-up velocity and it increases with the increase of the take-up velocity at the constant mass flow rate. This tendency is similar to that of maximum ASR as discussed above. This means that the higher the value of maximum ASR, the higher the value of tensile stress is. The simultaneous increase of both the tensile stress and maximum ASR leads to an increase in the deformation of filament. In other words, the filament deformation becomes more effective in both cases: decreasing the mass flow rate at the constant take-up velocity and increasing the take-up velocity for the constant mass flow rate.

Let us turn our attention back to the PLA morphologies in Figures 4 and 5, specially in Figure 4(d) (the last column on the right of the Figure 4) and Figure 5(a) (the first column on the left of the Figure 5). These PLA morphologies were obtained under the two special spinning conditions: (1) the highest mass flow rate $Q = 2.0$ g min^{-1} with the take-up velocity $v = 50$ m min^{-1}, (2) the lowest take-up velocity $v = 10$ m min^{-1} with the mass flow rate $Q = 1.0$ g min^{-1}. It is seen that the diameter of the PLA fibrils along the spinline in these two special spinning conditions decreases more slowly than that of other spinning conditions. The mean diameters of the PLA fibrils $\bar{d}$ in these spinning conditions are larger than that of other spinning conditions (Table III, Figure 10). Furthermore, the lengths of the PLA fibrils are not endless; they possess an average length of ca. 4–5 µm (Figure 11). This could be due to little coalescence or absence of coalescence and small deformation rate. In these two special spinning conditions, the maximum ASR has the lowest values. The maximum ASR for the mass flow rate $Q = 1.0$ g min^{-1} and take-up velocity $v = 10$ m min^{-1} is only ca. 1.23 s^{-1} (Table II and Figure 7). Furthermore, the tensile stress at the maximum ASR has also the lowest values, which are discussed and presented in Table II and Figure 9.

In contrast to the two above special spinning conditions, it is seen from Figure 4(a) (the first column on the left of Figure 4) and Figure 5(d) (the last column on the right of Figure 5) that the diameter of PLA fibrils more rapidly decreases along the spinline. These PLA fibrils were obtained under the two limiting spinning conditions (due to the stability of the melt spinning process, mass flow rates could not be decreased less than 0.5 g min^{-1} for a take-up velocity of 50 m min^{-1} and take-up velocity could not be increased more than 70 m min^{-1} for a mass flow rate of 1.0 g min^{-1}): (1) $Q = 0.5$ g min^{-1} and $v = 50$ m min^{-1};

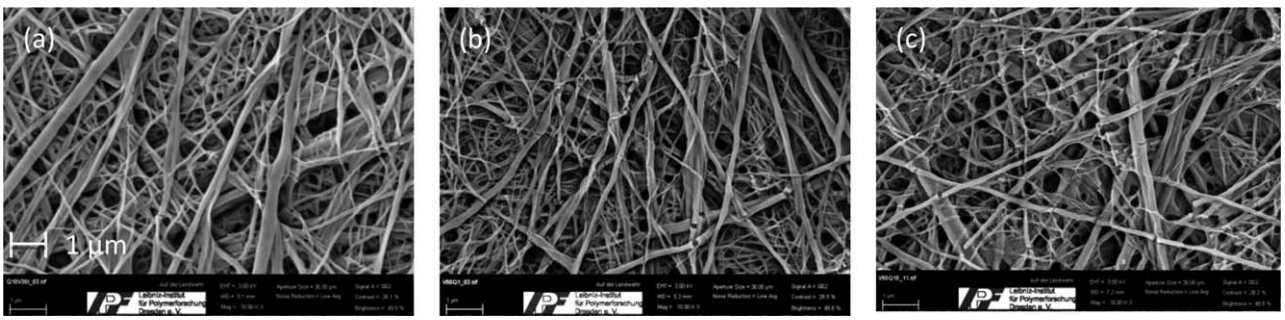

Figure 13. SEM images of the dispersed PLA phase from PLA/PVA-filaments at P8 for the last three spinning conditions: Q = 1.0 g min^{-1} and v = 30 m min^{-1} (a); Q = 1.0 g min^{-1} and v = 50 m min^{-1} (b); Q = 1.5 g min^{-1} and v = 50 m min^{-1} (c). Scale bar: 1 µm.

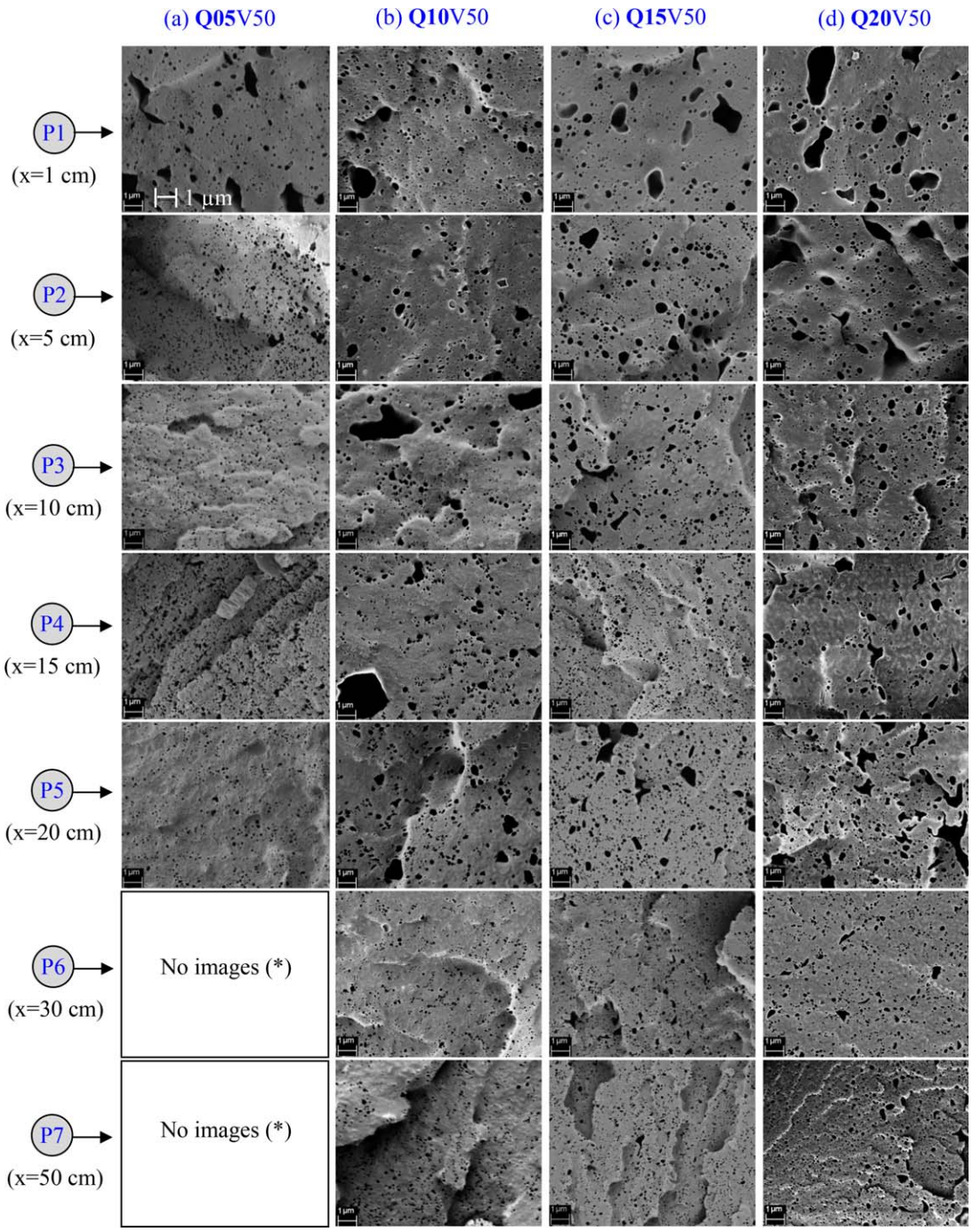

Figure 14. SEM images of cross-sectional PLA/PVA-filaments after etching the dispersed PLA phase for the various mass flow rates (0.5–2.0 g min^{-1}) (Q05–Q20) and the constant take-up velocity of 50 m min^{-1} (V50) (Q05V50, Q10V50, Q15V50, Q20V50) at different locations (P1–P7) along the spin-line: scale bar 1 µm, (*)Experiments were not done at this location because it was supposed that there is no difference in PLA morphology at this location with that at x = 20 cm (P5). [Color figure can be viewed at wileyonlinelibrary.com.]

(2) $Q = 1.0$ g min^{-1} and $v = 70$ m min^{-1}. The final diameters of PLA fibrils prepared using these limiting spinning conditions are much finer than that of other spinning conditions (Figures 10 and 12), especially in comparison with the PLA fibril diameters obtained using the above special spinning conditions (Figure 11). In these two limiting spinning conditions, the maximum ASR and the tensile stress at maximum ASR have the highest values in comparison with other spinning conditions: A maximum ASR ranging from ca. 9.1 to 10.6 s^{-1} (Table II and Figure 7) and a tensile stress at maximum ASR varying from 0.7 to 1.7 MPa (Table II and Figure 9). Like the PLA fibrils prepared using the two special spinning conditions, the length of PLA fibrils at the position P8 obtained using the two limiting spinning conditions appears to be also limited. However, it seems to be that these

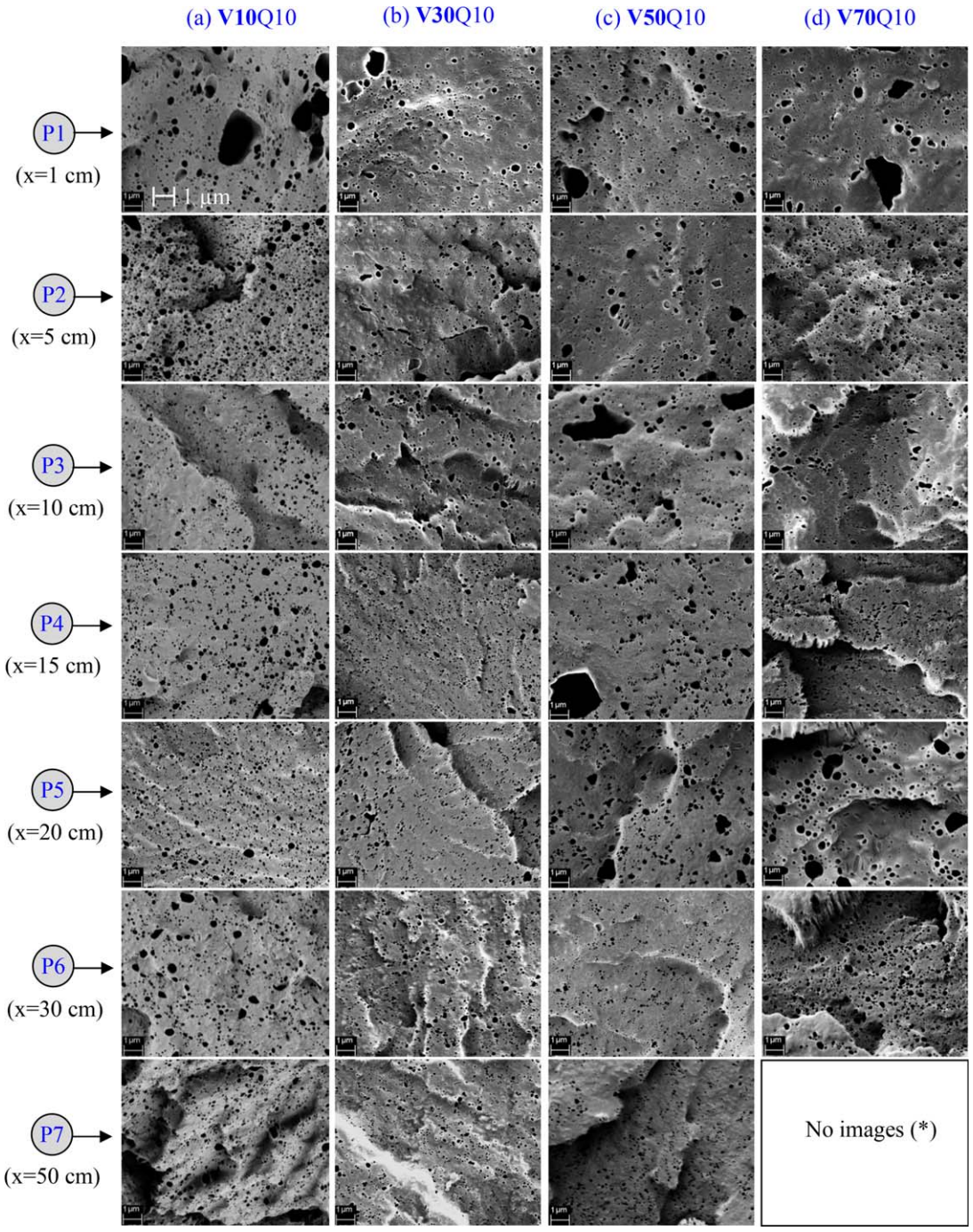

Figure 15. SEM images of cross-sectional PLA/PVA-filaments after etching the dispersed PLA phase for various take-up velocities (10–70 m min^{-1}) (V10–V70) and the constant mass flow rate of 1.0 g min^{-1} (Q10) (V10Q10, V30Q10, V50Q10, V70Q10) at different locations (P1–P7) along the spin-line: scale bar 1 μm, (*)Experiments were not done at this location because it was supposed that there is no difference in PLA morphology at this location with that at x = 30 cm (P6). [Color figure can be viewed at wileyonlinelibrary.com.]

very fine fibrils are connected together at their ends to form continuous fibrils, which is seen as a nanofibrous network (Figure 12). It is also seen from Figure 12 that a few of these very fine fibrils (ca. 30 nm in diameter) could have been broken-up after reaching their maximum deformation.

For the last three spinning conditions: (1) $Q = 1.0$ g min^{-1} and $v = 30$ m min^{-1}; (2) $Q = 1.0$ g min^{-1} and $v = 50$ m min^{-1}; (3) $Q = 1.5$ g min^{-1} and $v = 50$ m min^{-1}, in which the maximum ASR and the tensile stress at maximum ASR, respectively, vary over the range from ca. 2.6 to 7.7 s^{-1} (Table II and Figure 7) and from 0.35 to 0.52 MPa s (Table II and Figure 9). It is seen from Figure 13 that the remaining PLA fibrils after removing the PVA matrix at the position P8 have also limited lengths. However, like the PLA fibrils obtained using the two limiting

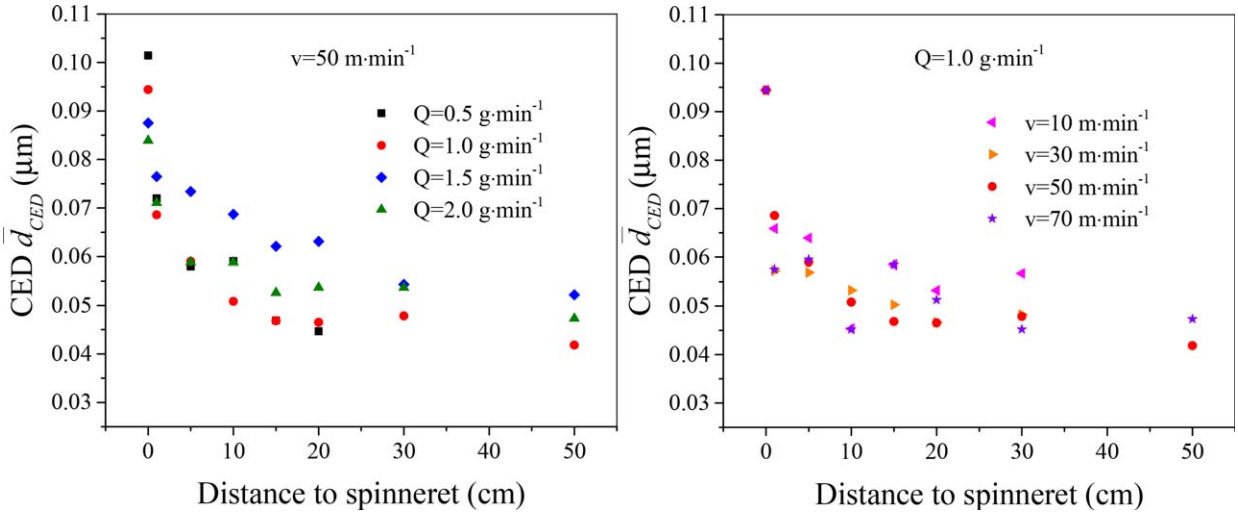

Figure 16. Mean CED $\bar{d}_{CED}$ of the dispersed PLA phase in cross-sectional PLA/PVA-filaments after etching the dispersed PLA phase vs. distance to spinneret. [Color figure can be viewed at wileyonlinelibrary.com.]

spinning conditions, most of the PLA fibrils seem to be joined each other at their ends to form longer fibrils, only a few very fine PLA fibrils with diameters less than ca. 50 nm are not connected together to form long continuous fibrils. It is also seen from Figure 13(c) that a few of these very fine fibrils could have been broken-up after reaching their maximum deformation.

From the above analyses of the morphological development of the remaining PLA phase from PLA/PVA-filaments after removing the PVA matrix and the filament profiles along the spinline, it can be said that the PLA morphology in PLA/PVA-filaments can be controlled by the changes in the spinning conditions, that are the changes in mass flow rates and/or take-up velocity, i.e. the variations of the ASR, maximum ASR, and of tensile stress. Under certain spinning conditions, the short PLA fibrils are deformed and coalescence to form the long continuous fibrils.

PLA Morphology in the Cross-sectional Surfaces of PLA/PVA-Filaments

Figures 14 and 15 demonstrate the SEM images of the PLA morphology in the cross-sectional PLA/PVA-filaments after etching the dispersed PLA phase at different locations (P1–P7) along the spinline for different spinning conditions. Figure 16 plots the mean circular equivalent diameter (CED) of the dispersed PLA phase versus distance to spinneret. Generally, like the mean diameter of the dispersed PLA phase $\bar{d}$ after removing the PVA matrix, the mean CED $\bar{d}_{CED}$ of the dispersed PLA phase after etching the PLA phase (Figure 16) decreases along the spinline for all spinning conditions. However, in some cases, it is seen that the mean CED $\bar{d}_{CED}$ along the spinline slightly increases after it initially decreases. The exact cause of this phenomenon is not known: we speculate that the reason is attributed to the radial coalescence of the neighbor PLA droplets through cross-section of PLA/PVA-filaments during the stretching process as schematically shown in Figure 17. Or this phenomenon could have occurred due to the imperfect fractured surfaces of the cross-sectional PLA/PVA-filaments and non-uniform fractured positions of PLA/PVA-filaments as discussed in our previous publication[6]. The latter reason is more acceptable than the former reason, because this phenomenon was not found for the dispersed PLA phase after removing the PVA matrix (Figure 6).

Comparing Figures 4 and 14, Figures 5 and 15, and Figures 6 and 16, an important observation can be found that many very fine PLA droplets/fibrils on fractured surfaces of the cross-

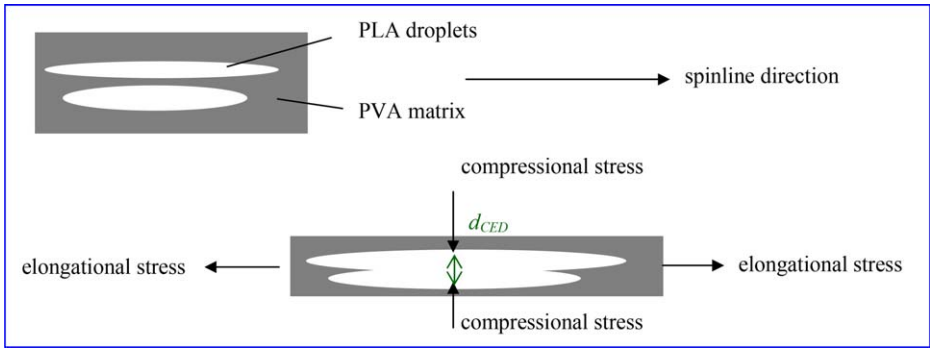

Figure 17. A schematic drawing of a possible radial coalescence of neighbor PLA droplets in a PLA/PVA- filaments during stretching process under effect of elongational and compressional stresses. [Color figure can be viewed at wileyonlinelibrary.com.]

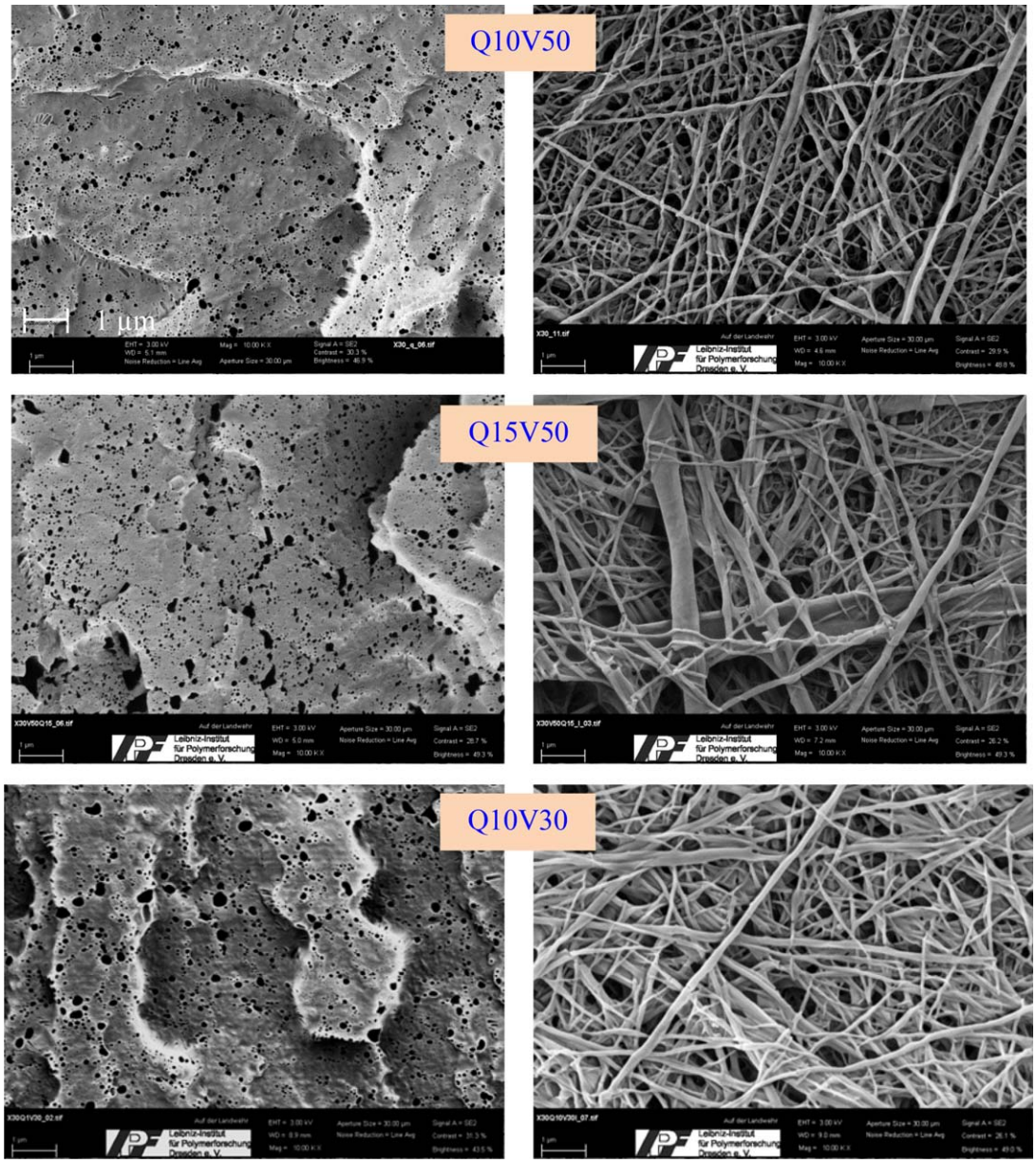

Figure 18. SEM images of PLA/PVA-filaments at position P6 (x = 30 cm) after removing the PVA matrix (right column) and etching the dispersed PLA phase (left column) for the last three different spinning conditions: Q = 1.0 g min^{-1} and v = 50 m min^{-1} (Q10V50); Q = 1.5 g min^{-1} and v = 50 m min^{-1} (Q15V50); Q = 1.0 g min^{-1} and v = 30 m min^{-1} (Q10V30), scale bar: 1 µm. [Color figure can be viewed at wileyonlinelibrary.com.]

sectional PLA/PVA-filaments after etching the dispersed PLA phase do not appear in the remaining PLA phase after removing the PVA matrix. Furthermore, the mean CEDs are always smaller than the mean diameters along the spinline ($\bar{d}_{CED} < \bar{d}$). Similar results have already been found for the PLA/PVA-extrudates without stretching as presented in our previous article.[6] To make this result clearer, the three pairs of the SEM images of PLA/PVA-filaments (Figure 18) at the position P6 ($x = 30$ cm) after removing the PVA matrix (images on the right column) and etching the dispersed PLA phase (images on the left column) from the last three spinning conditions are selected to analyze the diameter d and CED d_{CED} of PLA fibrils (Under these last three spinning conditions, the PLA droplets/fibrils seem to be more coalescent than other spinning conditions). Figure 19 gives the mean diameter $\bar{d}$ and the mean CED $\bar{d}_{CED}$ of the dispersed PLA fibrils. It is seen that the mean diameters are always larger than the mean CEDs for all the three selected spinning conditions $\bar{d} > \bar{d}_{CED}$. Furthermore, it is also obviously seen from Figure 20 that the cumulative number percentage of PLA droplets having diameter up to 0.1 µm was always more than that of PLA droplets having CED up to 0.1 µm. Especially for the spinning condition with $Q = 1.0$ g min^{-1} and $v = 30$ m min^{-1}, the difference of cumulative number percentage of PLA droplets between the diameter d and CED d_{CED} becomes larger: While there are ca. 72.1% the number of PLA droplets having CED up to 0.1 µm, there are up to 90% the

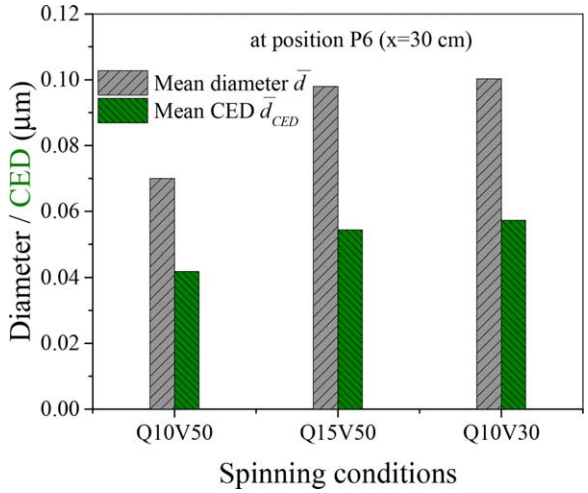

Figure 19. Mean diameter $\bar{d}$ and mean CED $\bar{d}_{CED}$ of the dispersed PLA phase from PLA/PVA-filaments at position P6 (x = 30 cm) for the last three different spinning conditions: Q = 1.0 g min^{-1} and v = 50 m min^{-1} (Q10V50); Q = 1.5 g min^{-1} and v = 50 m min^{-1} (Q15V50); Q = 1.0 g min^{-1} and v = 30 m min^{-1} (Q10V30). [Color figure can be viewed at wileyonlinelibrary.com.]

number of PLA droplets having diameter up to 0.1 µm. These results may allow one to confirm once again that most of very fine PLA droplets are removed together with the PVA matrix during removing process due to less or almost no coalescence among these very fine droplets or between them and other larger neighbor droplets.

Possible Conceptual Models of the Fibrillation Process of PLA/PVA-Filaments

Based on all the above analyses of the morphological development of the dispersed PLA phase and the profiles of PLA/PVA-filaments along the spinline, an overview of possible conceptual models of the deformation, coalescence, and break-up processes of the dispersed PLA droplets in PLA/PVA-filaments during melt spinning within fiber formation zone is summarized in Table IV and schematically visualized in more details in Figure 21. The possible conceptual models for the fibrillation process can occur in the following sequences, which are also summarized in Table V: the dispersed PLA droplets/fibrils are either deformed and no coalesced; or deformed and coalesced and further deformed; or deformed and coalesced and further deformed and broken-up along the spinline.

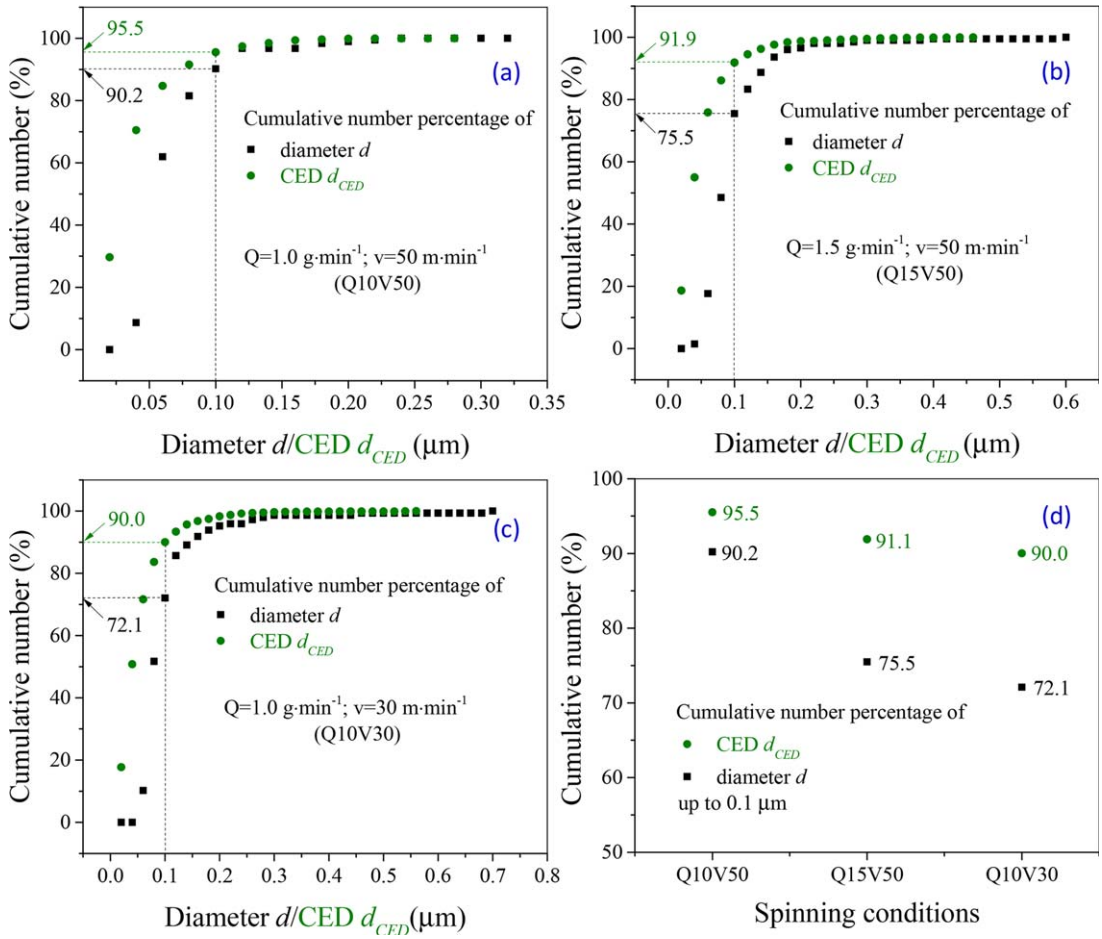

Figure 20. Cumulative number percentage vs. diameter d/CED dCED of the dispersed PLA phase from PLA/PVA-filaments at position P6 (x = 30 cm) for the last three different spinning conditions: (a) Q = 1.0 g min^{-1} and v = 50 m min^{-1} (Q10V50); (b) Q = 1.5 g min^{-1} and v = 50 m min^{-1} (Q15V50); (c) Q = 1.0 g min^{-1} and v = 30 m min^{-1} (Q10V30). (d) Cumulative number percentage of diameter d/CED dCED having diameter up to 0.1 µm. [Color figure can be viewed at wileyonlinelibrary.com.]

Table IV. An Overview of the Possibility of the Deformation (De), Coalescence (Co), and Break-up (Bu) Processes for Different Spinning Conditions

Spinning conditions (SCD)		
Group I (Two specific SCD)	Group II (Three last/middle SCD)	Group III (Two limiting SCD)
$Q = 1.0$ g min^{-1}; $v = 10$ m min^{-1}	$Q = 1.0$ g·min^{-1}; $v = 50$ m min^{-1}	$Q = 0.5$ g min^{-1}; $v = 50$ m min^{-1}
$Q = 2.0$ g min^{-1}; $v = 50$ m min^{-1}	$Q = 1.0$ g·min^{-1}; $v = 30$ m min^{-1}	$Q = 1.0$ g min^{-1}; $v = 70$ m min^{-1}
	$Q = 1.5$ g min^{-1}; $v = 50$ m min^{-1}	
Filament parameters		
Low max. ASR (1.2–2.3 s^{-1}) and low tensile stress	Middle max. ASR (2.6–7.7 s^{-1}) and middle tensile stress	High max. ASR (9.1–10.6 s^{-1}) and high tensile stress
The possibility of deformation, coalescence, and break-up		
Less deformation	More deformation	The most deformation
Less axial coalescence[a]	More axial coalescence	The most axial coalescence
No fibril break-up[b]	Almost no break-up	More break-up

[a] The coalescence in the direction along the spinline.
[b] Break-up for only the fibrils, which are formed after deformation and coalescence, not for the droplets.

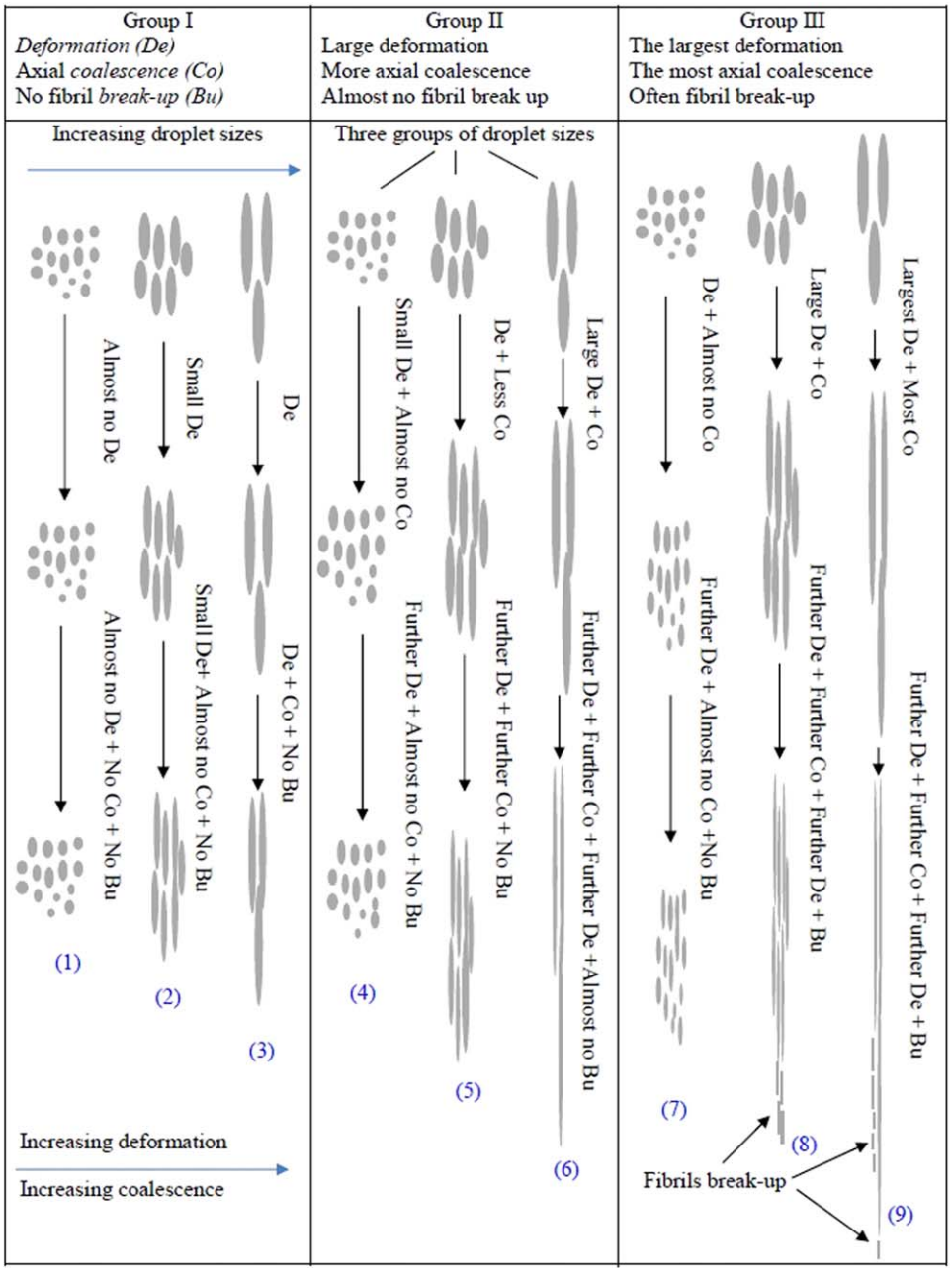

Figure 21. An overview of possible conceptual models of the deformation, coalescence, and break-up processes for different spinning conditions. [Color figure can be viewed at wileyonlinelibrary.com.]

Table V. Different Possible Sequences of Droplet Deformation, Coalescence, and Break-up

Sequences of deformation (De), coalescence (Co), and break-up (Bu)	Sequences number
De but no Co and no Bu	(1)
De and Co, but no Bu	(2) and (3)
De and Co, then further De and Co, but no Bu	(4), (5), and (7)
De and Co, then further De and Co, and then further De and Bu	(6), (8), and (9)

CONCLUSIONS

Owing to a new special self-constructed fiber capturing device at IPF Dresden, valuable insight was gained into the morphology development of the PLA/PVA-filaments within fiber formation zone under various spinning conditions. It was found that fibrillation process of the dispersed PLA phase from the rod-like to nanofibrillar structures mainly occurs in the fiber formation zone under the effect of an elongational flow. In this zone, the PLA/PVA-filaments were converted from the molten to viscoelastic state; the filament velocity and tensile stress increased rapidly.

The final sizes of PLA fibrils were controlled by changes in the spinning conditions via the take-up velocity and flow rate. The final diameter of PLA fibrils become finer as the mass flow rate decreases for the constant take-up velocity or as the take-up velocity increases for the constant flow rate. The deformation, coalescence, and break-up of the dispersed PLA phase depend on the spinning conditions via the value of maximum ASR and the tensile stress. It is shown that the higher the value of maximum ASR and tensile stress at maximum ASR, the more the PLA fibrils deform and coalesce. However, if the maximum ASR and tensile stress at maximum ASR reach their upper limit values of ca. 9 s^{-1} and 1.7 MPa, respectively, the break-up of the deformed and coalesced PLA fibrils with a very fine diameter (ca. 30 nm) occurs. On the contrary, if the maximum ASR and tensile stress at maximum ASR have lower values of 1.23 s^{-1} and 0.26 MPa, respectively, the coalescence process almost does not occur. The lengths of PLA fibrils are not endless; they possess an average length of ca. 4–5 μm. It is suggested that the optimal spinning conditions for the formation of long continuous PLA fibrils in PLA/PVA-filaments should be processed with the maximum ASR range from ca. 3 to 9 s^{-1}

Another major contribution of the present work was that the analysis of the morphological development of the dispersed PLA phase in PLA/PVA-filaments along the spinline were done in the both cross-sectional and longitudinal direction of PLA/PVA-filaments: the PLA fibrils after removing the PVA matrix and the remaining holes of PLA fibrils in cross-sectional PLA/PVA-filaments after etching the dispersed PLA phase were simultaneously studied. The results demonstrated that there is almost no axial coalescence between small PLA droplets/fibrils during stretching of PLA/PVA-filaments within fiber formation zone. In contrast, the big droplets/fibrils are well deformed and coalesced in an elongational flow under the effect of the ASR and the tensile stress. The deformed and coalesced fibrils of the above mentioned big droplets/fibrils are further deformed. They reach a lower critical diameter of ca. 30 nm. And they will then break-up into short thin fibrils if the maximum ASR is higher than its critical value in combination with the high tensile stress. Finally, possible conceptual models for the fibrillation process of the dispersed PLA phase were proposed depending on the spinning conditions and the droplet sizes.

ACKNOWLEDGMENTS

Authors would like to thank for the financial support of the German Research Foundation within the research project „ Entwicklung eines neuartigen Filamentgarnes “(BR 1886-/6-1). Authors are very grateful to Mr. Norbert Smolka and Mr. Mathias Häschel for their kind assistance with numerous melt spinning experiments. Nguyen Hoai An Tran gratefully thanks the Vietnamese Ministry of Education and Training for a doctoral scholarship.

APPENDIX

Deformation of PLA Droplet

Figure A.1 presents comparison between the measured mean diameter $\bar{d}$ of the dispersed PLA phase after removing the PVA

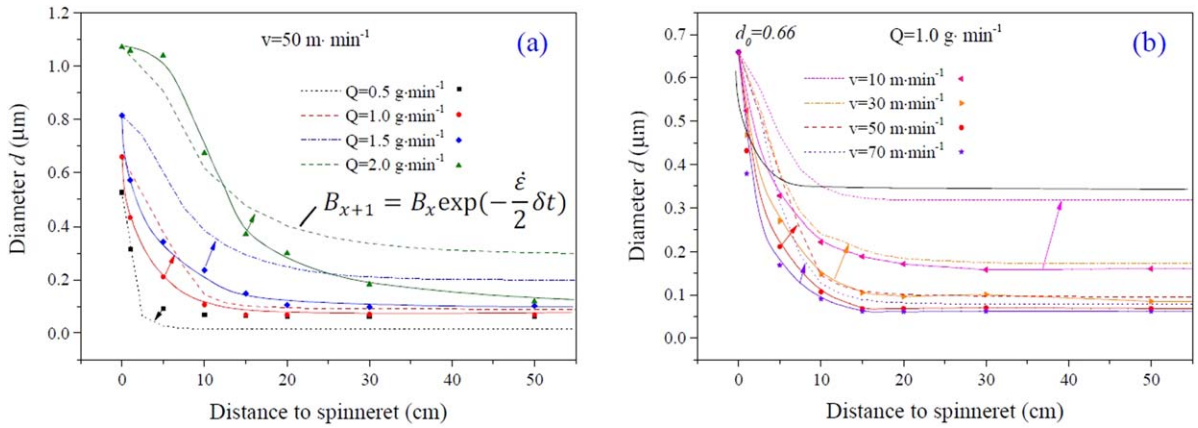

Figure A.1. Comparison between the calculated diameters B (dash curves) of the PLA droplets/fibrils after affine deformation theory and the measured mean diameters d (continuous curves) of the PLA phase after removing the PVA matrix: (a) v = 50 m min^{-1}; Q = 0.5, 1.0, 1.5, and 2.0 g min^{-1}; (b) Q = 1.0 g min^{-1}; v = 10, 30, 50, and 70 m min^{-1}. [Color figure can be viewed at wileyonlinelibrary.com.]

matrix and the calculated diameter B of the dispersed PLA phase using the affine deformation theory after eq. (A.1):

$$B_{x+1} = B_x \exp\left(-\frac{\dot{\varepsilon}}{2}\delta t\right) \quad \text{(A.1)}$$

where, $\dot{\varepsilon}$ is the local average elongation rate $\dot{\varepsilon} = \delta v(x)/\delta x$ and δt is the period of time within $\delta x = 2.5$ cm along the spinline.

It is seen that the calculated diameter B of PLA phase using the affine deformation theory and the measured diameter d of PLA phase after removing PVA matrix could not be well fitted together.

In principle, the calculation of PLA droplet deformation was calculated using the affine deformation theory with an assumption that PLA droplets/fibrils have cylindrical shapes with their volume being conserved in non-isothermal melt spinning process. Furthermore, the affine deformation theory is only appropriate for small deformations and for a few droplets, in which all droplets have the same droplet size.

Therefore, it can be concluded that the affine theory are not applicable for the PLA droplet deformation in PLA/PVA-filaments along the spinline, because the distribution of PLA droplets is very broad as discussed in our previous publication.[6] All the droplets could not be counted during calculating using the affine deformation theory.

REFERENCES

1. Padsalgikar, A. D.; Ellison, M. S. *Polym. Eng. Sci.* **1997**, *37*, 994.
2. Yang, J.; White, J. L.; Jiang, Q. *Polym. Eng. Sci.* **2010**, *50*, 1969.
3. Tavanaie, M. A.; Shoushtari, A. M.; Goharpey, F.; Mojtahedi, M. R. *Fiber Polym.* **2013**, *14*, 396.
4. Tran, N. H. A.; Brünig, H.; Boldt, R.; Heinrich, G. *Polymer* **2014**, *55*, 6354.
5. Tran, N. H. A.; Brünig, H.; Heinrich, G. *J. Appl. Polym. Sci* **2016**, DOI:10.1002/APP.44258.
6. Tran, N. H. A.; Brünig, H.; Auf der Landwehr, M.; Vogel, R.; Pionteck, J.; Heinrich, G. *J. Appl. Polym. Sci* **2016**, DOI: 10.1002/APP.44257.
7. Kase, S.; Matsuo, T. *J. Polym. Sci. Part A: Gen. Papers* **1965**, *3*, 2541.
8. Ishibashi, T.; Aoki, K.; Ishii, T. *J. Appl. Polym. Sci.* **1970**, *14*, 1597.
9. Oh, T. *Polym. Eng. Sci.* **2006**, *46*, 609.